Construction Method of a Guaranteed Grid Considering the Specific Recovery Process

Shengfeng Zhang [1], Jie Zhao [1,*], Yixuan Weng [2], Dichen Liu [1], Weizhe Ma [2] and Yuhui Ma [1]

[1]   School of Electrical Engineering and Automation, Wuhan University, Wuhan 430072, China;
      sf-zkinjaz@whu.edu.cn (S.Z.); dcliu@whu.edu.cn (D.L.); 805610381myh@whu.edu.cn (Y.M.)
[2]   Shenzhen Power Company Ltd., Shenzhen 518001, China; liuqioscar@whu.edu.cn (Y.W.);
      2014302540094@whu.edu.cn (W.M.)
*   Correspondence: jiez_whu@whu.edu.cn

Abstract: For the planning of the guaranteed power grid, only the operation capacity of the target grid is considered. The recovery process and steps of the backbone grid are not considered enough, which leads to two defects: the minimum guaranteed power grid is not conducive to the unit recovery and the recovery time is too long. In this paper, a method of constructing the grid with the specific recovery process is proposed. Considering the influence of the grid structure and the position of the black start power supply on the recovery steps, the recovery success rate and the recovery time of the grid, the optimization of the grid structure of the guaranteed grid can meet the demand of power supply and at the same time make the recovery of the target grid less time-consuming and achieve a higher recovery success rate in the event of a blackout. In this method, two aspects are considered: the power failure recovery scenario in the recovery process of the target grid and the normal power supply scenario, reflecting the power supply performance after the recovery of the target grid. In the normal power supply scenario, a three-objective optimization model including power supply capacity, smooth transmission and safety margin is constructed, with power supply capacity and safe operation as constraints. In the scenario of power failure recovery, the process of power grid recovery and the mechanism affecting the success of recovery are analyzed to form the line recovery index. The Dijkstra algorithm is used to search for the optimal recovery path and calculate the recovery index, so as to reoptimize the backbone power grid. The validity of the method is verified by standard and practical examples.

Keywords: recovery path; guaranteed grid; multi-objective optimization; system recovery; optimization algorithm

1. Introduction

At present, the construction of the guaranteed power grid for strengthening the important load power supply is an important issue in typhoon-prone areas, ice waterlogging and heavy load concentrated areas along the coast [1]. With the expansion of the power grid, the complexity of the structure and the frequent occurrence of disasters, blackouts often occur [2–5]. If the backbone grid of the guaranteed grid cannot be successfully restored in a short time in the event of power failure, it will cause huge losses to the social economy [4,5]. At the same time, the important load and the unit with strong power generation capacity selected by the backbone grid frame of the guaranteed power grid in the normal scenario will take too much time or even fail to recover due to the tedious recovery steps in the outage scenario [6–10]. Therefore, it is of great significance to study the construction method of a backbone grid structure considering the recovery ability for the reliable recovery of the grid structure and the reduction of the outage time of important load in the outage scenario. In this paper, combined

with the specific recovery process leading to recovery failure and the key factors determining the recovery time, we extract quantitative indicators for optimization planning and optimize the backbone grid structure of the bottom guaranteed grid, to make the recovery operation less prone to fail after a blackout and reduce the time consumed by the grid from the blackout to the recovery of power supply. In this way, we can guarantee the power supply of important loads more comprehensively.

At present, scholars at home and abroad are following two main research directions with regard to the backbone grid of the guaranteed grid. One is to improve the search efficiency of the target grid in the multi-node high latitude grid from the solution algorithm [11–15]; the other is to construct the appropriate objective function to adapt to the trend of increasing the ratio of new energy, expanding the scale of the grid. The research focuses on improving the new energy consumption of the backbone grid of the guaranteed grid, the proportion of important load and the disaster resistance [16–25], but the research to ensure the power grid recovery capacity is not sufficient. The current elastic recovery index of grid is based on the importance of load and network structure, not specifically combined with the recovery plan, to quantify the recovery time and recovery success rate. In Gu et al. and Dong et al. [16,17], based on the economic benefits of the load and the transmission capacity of the line, the recovery sequence of the line and nodes is determined to improve the elastic recovery capacity, but the difficulty and time consumption of the line and nodes in the recovery operation are not considered. Zhu et al. and Feng et al. [18,19] analyze the optimization of the unit start sequence and start path in the process of recovery of the backbone grid structure of the minimum guaranteed power grid. The authors clarify the mechanism of recovery failure caused by key equipment parameters but do not form the index to guide the backbone grid structure planning of the guaranteed power grid. In Zhao et al. [20], based on the node importance analysis method, the importance of new energy and the network cohesion of the reaction grid structure are highlighted in the analysis of the power supply importance, but the starting difficulty and the power generation capacity provided by the electric generating unit in the recovery process are ignored. In Huan et al. [21], when considering the importance of the line, the cables with less impact of wind disaster are highlighted to improve the proportion of cables in the grid structure. In Zhou et al. [22], based on the survival rate index of the line under a disaster, the backbone grid structure with strong resistance to disasters is searched. The above-mentioned documents do not consider the factors that lead to recovery failure due to line overvoltage. In Bi et al., Golshani et al. and Fu et al. [23–25], the backbone grid is constructed based on the voltage, power margin and important load coverage during operation. The backbone grid structure that is easier to restore is not considered.

To sum up, the optimization of the backbone grid structure of the minimum guaranteed power grid involves the energy supply of the important loads under the normal scenario and the recovery capability under the blackout scenario. The existing optimization model of the backbone grid structure of the minimum guaranteed power grid improves the power supply capability mostly under the normal scenario from the important load coverage, new energy consumption and operation stability of the grid. In the case of power failure, the research is insufficient. The existing method only quantifies the recovery index based on the importance of the load and network structure, and does not analyze the actual recovery steps and key factors such as black start power supply and the equipment parameters that affect the recovery effect. Based on the normal scene optimization model, this paper analyzes the recovery steps and key factors, quantifies the recovery time and the recovery success rate of the grid, increases the recovery index, optimizes the conventional multi-objective backbone grid optimization scheme, improves the recovery success rate and shortens the recovery time.

2. Overall Research Framework

The construction of the core backbone grid structure of the minimum guaranteed power grid is considered from two aspects: the normal power supply scenario and the power failure recovery scenario. In the normal scenario, the power supply capability and risk resistance capability of the grid

structure are optimized. In the power failure scenario, the grid structure is improved to increase the grid recovery capability. The overall scheme is shown in Figure 1.
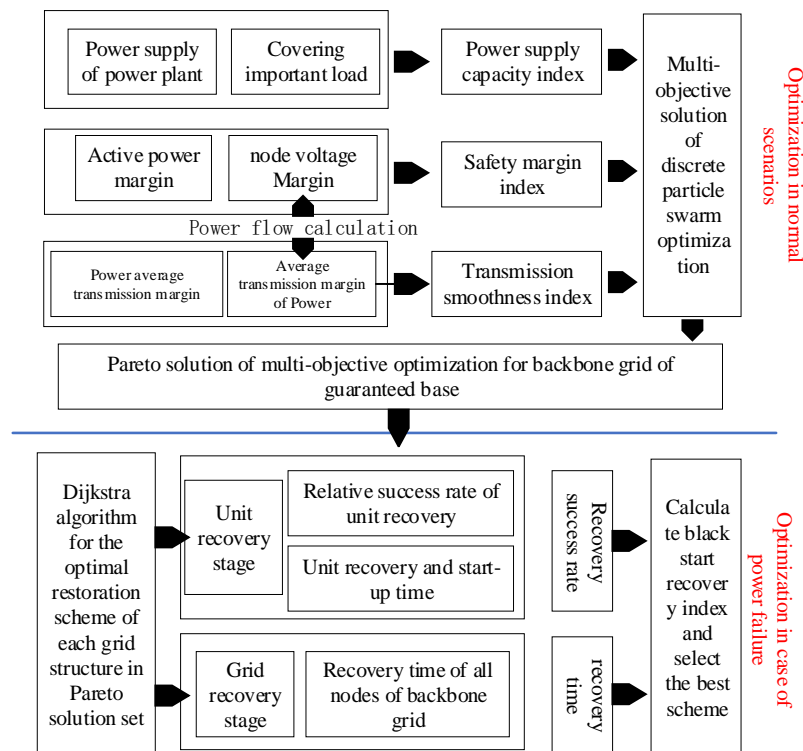
Figure 1. The framework of the backbone grid structure considering the recovery ability.
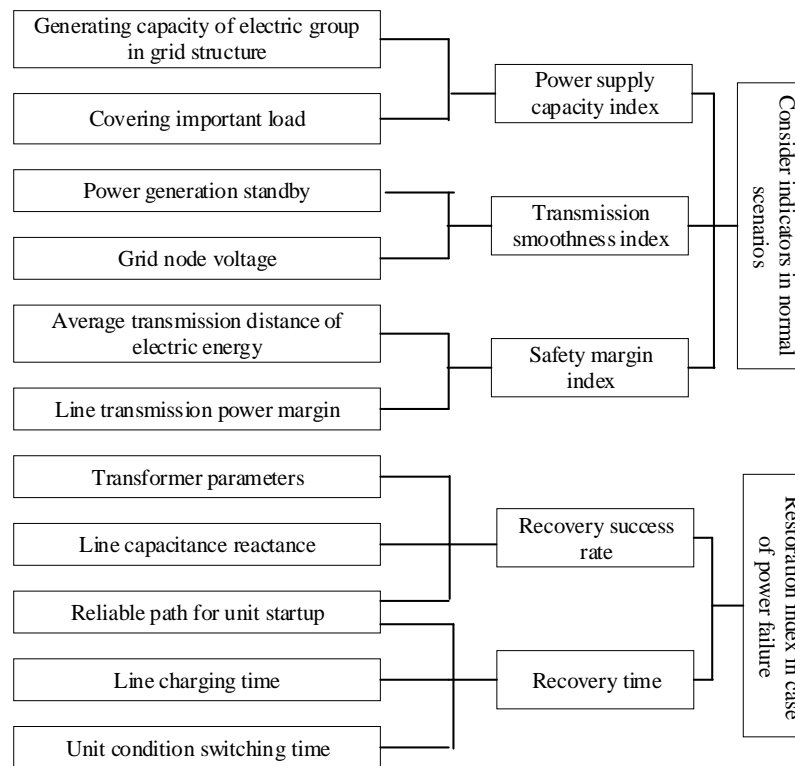
In the normal scenario, the backbone grid is optimized from three objectives—power supply capacity, safety margin and smooth transmission:

(1) The power supply capacity is reflected in that the backbone grid should be able to meet the important load demand, so the grid should select the access to the important load according to the load and the user's importance level. At the same time, sufficient power supply should be reserved in order to ensure the power balance.

(2) The smooth transmission reflects the difference between transmission power and the upper limit of transmission power in the electric wire. The load in the grid is largely reserved. In contrast to load retention, the backbone grid lines are greatly reduced, which leads to the increase of line burden and the extreme occurrence of power flow overrun and transmission congestion.

(3) The ample safety margin aims to ensure that the backbone grid can operate stably for a period of time. When the active and reactive power in the backbone grid is sufficient, the system has a strong ability to deal with sudden small disturbances. Therefore, the safety margin is quantified as the margin between the electrical quantity and the limit operation state.

In the case of power failure, the reliability and recovery time of the backbone grid are fundamentally determined by the grid topology and the location of the generator set in the grid topology. The proper core backbone grid structure can make the black start power supply go through fewer lines and equipment to restore the plant's power, so the recovery success rate is higher when the start success rate of each equipment is certain. Therefore, the recovery time and recovery success rate of the backbone grid are selected to form the black start recovery index f_{rec}, by which the Pareto non-dominated solution set obtained from the normal scene is reoptimized. Therefore, the backbone grid structure can not only have the power supply capacity, smooth transmission and safety margin under normal scenarios, but also recover quickly and reliably after a blackout.

3. Optimization Model of the Backbone Grid Structure with Recovery Capability

The objective function considerations in the normal power supply scenario and the power failure recovery scenario are shown in Figure 2. The calculation of the power supply capacity, transmission smoothness, safety margin and recovery index in this paper are based on the parameters involved in Figure 2.

Figure 2. Objective function considerations.

3.1. Optimization of the Backbone Grid Structure in the Normal Scenario

3.1.1. Objective Function

The optimization objective function of the backbone grid in the normal energy supply scenario is shown in Equation (1).

$$F_{normal} = \max(f_1, f_2, f_3) \tag{1}$$

Power Supply Capacity Index f_1

The power supply capacity index reflects the relative load and power conservation of the backbone grid of the guaranteed base grid, which can be expressed as Equation (2).

$$f_1 = a_1 + \beta_1 a_2 \tag{2}$$

a_1, a_2 have been standardized and are in the same order of magnitude. When $\beta_1 > 1$, compared with the power supply, the grid structure prioritizes the retainment of the important load. Otherwise, it focuses more on the power node and voltage margin. Considering that the power supply and load should meet the power balance constraints, $\beta_1 = 1$ is in line with the actual operation.

a. Power saving rate a_1

Power saving rate can be shown in Equation (3).

$$a_1 = \sum_{k=1}^{b_g} w_k^{bg} / \sum_{i=1}^{n_g} w_i^{ng} \tag{3}$$

where w_k^{bg} is the rated generation capacity of the k generation node in the grid; and w_i^{ng} is the rated generation capacity of the generation node in the grid before optimization.

b. Important load preservation rate a_2

Important load preservation rate can be shown in Equation (4).

$$a_2 = \sum_{k=1}^{b_l} \alpha_k w_k^{bl} / \sum_{i=1}^{n_l} \alpha_i w_i^{nl} \tag{4}$$

where w_k^{bl} is the power consumption of the k load node in the grid; and w_i^{nl} is the rated power generation of the i power generation node in the grid before optimization.

Safety Margin Index f_2

According to Liu et al. [6], the concept of margin expresses the distance between the specific value of a certain parameter and the limit value specified by the parameter. In mathematics, the following expression is shown in Equation (5).

$$M_x = (x_{\max} - x^{\max}) / x_{\max} \tag{5}$$

where $x_{\max}$ is the upper limit specified for the parameter; M_x is the margin of the parameter x; and $x^{\max}$ is the maximum value of the parameter x in a period of time scale.

The safety margin index reflects the reliability of the backbone grid during operation, which is quantified as the margin between the electrical quantity and the limit operation state. It can be expressed as Equation (6).

$$f_2 = s_1 + \beta_2 s_2 \tag{6}$$

In the calculation of the node voltage margin s_1 and the power margin of power generation node s_2, a standardized treatment is made. s_1 and s_2 are all in the same order of magnitude. When $\beta_2 > 1$, compared with the node voltage margin, the grid structure pays more attention to the node power margin; Otherwise, it pays more attention to the voltage margin. β_2 can be selected between 0.5 and 1.5 according to actual demand.

a. Node voltage margin s_1

Node voltage margin can be shown in Equation (7) and Equation (8).

$$s_1 = \sum_{k=1}^{b} r_k^b \times U_k^* \tag{7}$$

$$U_k^* = \begin{cases} \dfrac{U_k - U_{kN}}{U_{\max.k} - U_{kN}} & U_k > U_{kN} \\[2ex] \dfrac{U_{kN} - U_k}{U_{kN} - U_{\min.k}} & U_{kN} > U_k \end{cases} \tag{8}$$

where U_{kN} is the rated voltage of the k node; $U_{\max,k}$ is the upper limit of the allowable voltage of the k node; and $U_{\min,k}$ is the lower limit of the allowable voltage of the k node.

b. Power margin of the generating node s_2

During the operation of the backbone grid frame of the minimum guaranteed power grid, a certain power generation margin shall be reserved under the conditions of equipment maintenance, accident, frequency modulation, etc., to meet the demand of the power market. The equation to calculate the power margin of the generating nodes is shown in Equation (9).

$$s_2 = \sum_{k=1}^{bg} \left(\frac{w_i^{bg}}{\sum_k^{bg} w_k^{bg}} \times \frac{w_{i,\max}^{bg} - w_i^{bg}}{w_{i,\max}^{bg}} \right) \tag{9}$$

where $w_{i,\max}^{bg}$ is the maximum active power output of the i generation node in the grid structure.

Transmission Smoothness Index f_3

The electricity smoothness index reflects the margin of transmission active power on each transmission path when the backbone grid is running, which can be shown in Equation (10) and Equation (11).

$$f_3 = \sum_{k=1}^{n_{path}} r_k^{path} (P_{k,\max}^{path} - P_k^{path}) / P_{k,\max}^{path} \tag{10}$$

$$r_k^{path} = \frac{P_{k,\max}^{path}}{\sum_{i=1}^{n_{path}} P_{i,\max}^{path}} \tag{11}$$

where r_k^{path} is the weight of the k line in the grid; $P_{k,\max}^{path}$ is the active power transmission limit of the k line in the grid; and P_k^{path} is the active power transmission of the k line in the grid in the normal power supply scenario.

3.1.2. Multi-Objective Optimization Solution

In the normal power supply scenario, the optimization of the backbone grid is a multi-objective optimization problem. In this paper, the discrete particle swarm optimization (DPSO), which has a strong global convergence ability and good robust performance, is used to solve the model in the normal scene. The solution algorithm flow is shown in Figure 3.

The key steps are as follows:

(1) When initializing a particle swarm $X = (X_1, X_2, \cdots, X_n)$, the position coordinate of each individual in the particle swarm is $X_i = (x_{i1}, x_{i2}, \cdots, x_{id})$; dimension d is equal to the number of branches of the original grid. In the discrete particle swarm algorithm, the value of each dimension of the position variables of all particles x_{ik} is limited to 0 or 1.

(2) According to Lin et al. [26], the speed and position of the particles are updated according to Equations (11) and (12), respectively:

$$v_{id}^{k+1} = w v_{id}^k + c_1 r_1 (p_{id}^k - x_{id}^k) + c_2 r_2 (p_{gd}^k - x_{id}^k) \tag{12}$$

$$x_{id}^{k+1} = x_{id}^k + v_{id}^{k+1} \tag{13}$$

(3) Check the validity of the updated particles. Because this is a graph theory problem, we must judge the connectivity of the branch and node set corresponding to the particle position. If it is connected, it is an effective particle—go to step 4); If it is not connected, it is an invalid particle—go back to step 2) after transforming the invalid particle.

(4) According to the particle position, we can determine the branch, node set and grid structure. After the power flow calculation, the node voltage and power flow distribution are obtained.

Judge whether the constraints of a safe and stable operation of the power system are met. If so, go to step 5). Otherwise, return to step 2) and regenerate new particles.

(5)　According to the results of the power flow calculation and basic data, the fitness function value is calculated by the optimization objective function of Equation (1), so as to update the particle optimal position and particle swarm optimal position.

(6)　If the number of iterations is reached, the iteration is terminated and the result of the grid optimization, which is the non-dominated solution set of grid Pareto with strong transmission capacity and full reliability. Otherwise, skip to step 2) and continue to perform the particle update.
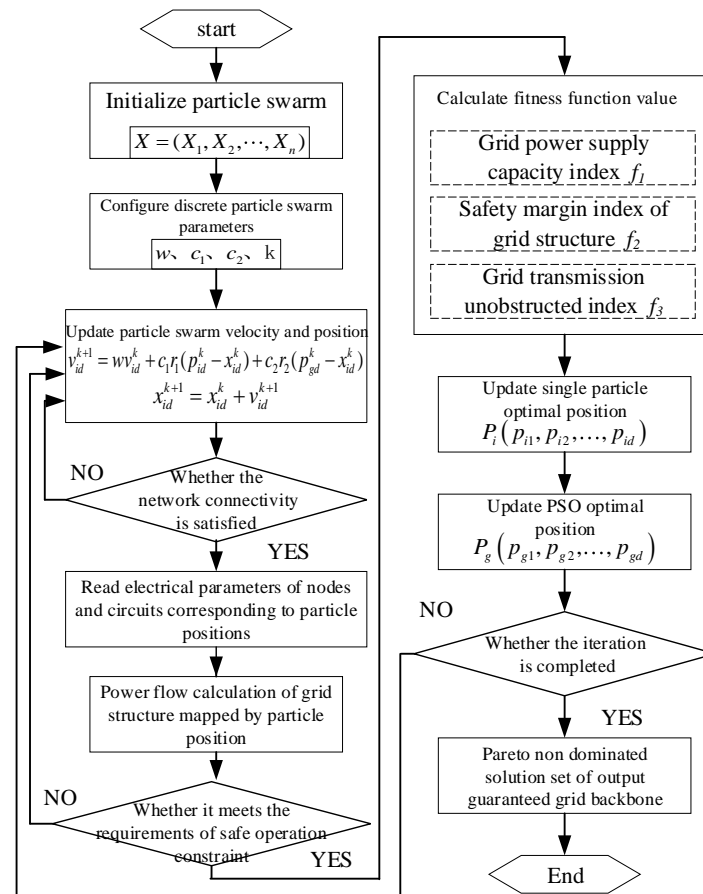
Figure 3. Algorithm flow of core backbone grid optimization in the normal power supply scene.

3.2. Re-Optimization Based on the Recovery Capability in the Outage Scenario

3.2.1. Objective Function Considering the Recovery Ability of the Grid Structure

In the normal scenario, the Pareto non-dominated solution set considering the power supply capacity, smooth transmission and safety margin is obtained. Then, the grid restoration capacity is introduced to optimize the second stage in the outage scenario. The objective function is shown in Equation (14).

$$F_{black} = \min f_{rec} \tag{14}$$

Considering the recovery time and recovery success rate of the grid structure, recovery indicators can be shown in Equation (15).

$$f_{rec} = f_{able} - \beta_3 T \tag{15}$$

The calculation of f_{able} and T is based on the two steps in the recovery stage of the whole backbone grid [21]. The first step is that the black start unit in the grid starts automatically to provide power

support to the unit that cannot be started in the grid, so that it can start. The second step is to restore the load nodes in the grid after the backbone grid has sufficient power generation capacity. Among them, the first step of the recovery process mainly determines the recovery success rate f_{able}. In case the generator set has not been started, the active and reactive power in the system are not sufficient. At this stage, the grid structure is relatively fragile. The disturbance in the process of charging the no-load line and putting the no-load transformer into operation may cause the failure of the core backbone grid structure recovery. The recovery time T shall include the start-up time of the first step and the remaining line and node of the second step consumption time.

Recovery Success Rate Fable f_{able}

Recovery can be shown in Equation (16).

$$f_{able} = \max_{L_i \in \Phi}(W_{L_i} \times \prod_{T_k \in L_i} W_{T_k}) \tag{16}$$

a. Line index W_{Li}

The expression of line charging overvoltage in Liu et al. [6] is recovery indicators can be shown in Equation (17).

$$u_g = \frac{E}{\cos \alpha l - \frac{X_s}{Z_c} \sin \alpha l} \tag{17}$$

According to the charging overvoltage expression (17), it can be seen that the line parameter affecting the line overvoltage amplitude is the equivalent capacitive reactance, so the line index expression is recovery indicators can be shown in Equation (18).

$$W_{L_i} = \prod_{j=1}^{n} \frac{1}{\frac{X_{Cmax}}{X_{Cj}}} \tag{18}$$

b. Transformer index W_{T_k}

The expression of line charging overvoltage in Liu et. al [6] is recovery indicators can be shown in Equation (19).

$$i = N_1 \frac{\phi_{mk} \sin(wt + \alpha) + (\phi_{satk} - \phi_{mk} \sin \alpha)e^{-\frac{R}{L}t}}{L} \tag{19}$$

According to the charging over-voltage expression, it can be seen that the line parameter affecting the line overvoltage amplitude is the equivalent capacitive reactance, so the line index expression is recovery indicators can be shown in Equation (20).

$$W_{T_k} = \frac{\phi_{satk} - \phi_{resk}}{\phi_{mk}} \tag{20}$$

where ϕ_{satk}, ϕ_{resk} and ϕ_{mk} are the saturation flux, residual flux and steady flux of the transformer.

Recovery Time T

The recovery time can be shown in Equation (21).

$$T = T_1 + T_2 \tag{21}$$

Since multiple units are started through multiple paths, the first-stage recovery time is selected as the maximum time required for the path in path set. The first-stage recovery time can be shown in Equation (22).

$$T_1 = \underset{L_i \in \Phi}{MAX}(\sum_{j \in L_i} t_j^L + \sum_{G_k \in L_i} t_k^G) + t_{black} \tag{22}$$

The time required for the second step of the system recovery mainly considers the recovery time of all the lines and the climbing time of the unit power. The time required for the second step of the system recovery can be shown in Equation (23).

$$T_2 = \sum_{j \in L_{max}} t_j^L + MAX(\frac{w_1^{bg}}{P_1^G}, \cdots, \frac{w_k^{bg}}{P_k^G}, \cdots, \frac{w_m^{bg}}{P_m^G}) \tag{23}$$

3.2.2. Optimal Recovery Path

As shown in Figure 4, when the position of the black start unit and the started unit in the grid is determined, there may still be multiple path connections. Therefore, when calculating the objective function of the power failure recovery scenario, in addition to searching for the longest path of recovery time, it is also necessary to search for the highest path of recovery success rate for each grid unit in the Pareto non-dominated solution set.
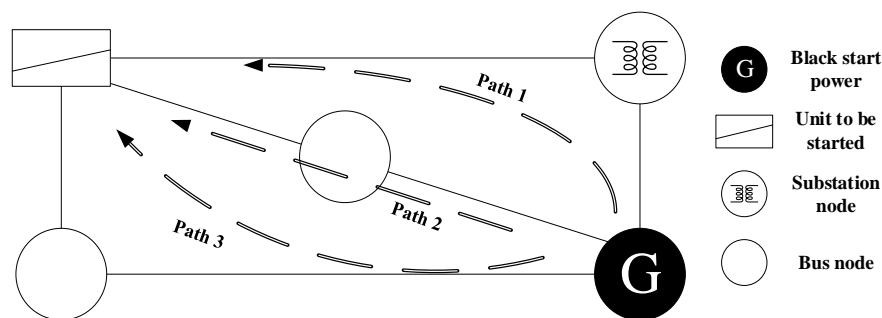

Figure 4. Multipath between unit to be started and black start power supply.

Based on the typical shortest path algorithm Dijkstra, the improved algorithm searches for the path with the highest recovery success rate and the path with the longest recovery time. The Dijkstra algorithm calculates the distance by adding the length of the line. However, the recovery success rate index is multiplication. Therefore, when searching for the path with the highest recovery success rate, the logarithmic method is used to convert multiplication to summation. The line length is shown in Equation (24).

$$q_i = \ln \frac{X_{Cj}}{X_{Cmax}} + \ln W_{Ti} \tag{24}$$

When searching for the path with the longest recovery time, the path with the highest recovery success rate has been searched for, and the corresponding time can be calculated. It mainly searches for the path with the longest recovery time from the line and node involved in the starting unit to the unrecovered node. When the Dijkstra algorithm is used to search, the recovery time of the line and the equipment is taken as the line length. However, it is inefficient to calculate the number of nodes that have not been recovered to the number of nodes that have been recovered. Therefore, the equivalent node idea is used to simplify. The principle is shown in Figure 5. The envelope line is drawn to include all the recovered lines and nodes. Then, the nodes and lines that are circled in are equivalent to an initial node. The lines cut from the envelope line and the nodes at the other end of the line are connected with the initial node, and the rest of the network frame is unchanged. At this time, only the distance from the rest of the nodes to the initial node is calculated.
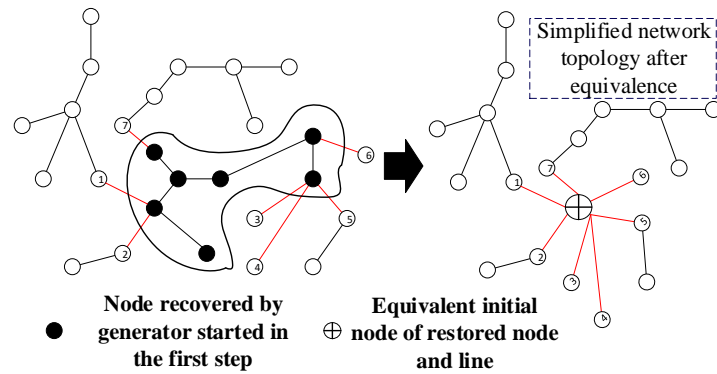
Figure 5. Equivalent node of recovered node and line set.

To sum up, the Dijkstra algorithm is used to solve the optimal recovery scheme in the blackout scenario as follows:

(1)   Extract a network topology map of a grid in Pareto's non-dominated solution set. Assign the sum of the inverse number of transformer exponents at both ends of the line and the unit value of capacitive reactance of the line itself as the line length. The Dijkstra algorithm searches for the shortest path. Calculate f_{able} and T_1 according to the path.

(2)   Confirm that the nodes and lines involved in the optimal path are equivalent to the initial nodes. The sum of the recovery time of the line and the equipment at both ends of the line is assigned as the line length. The Dijkstra algorithm searches for the farthest path and calculates T_2.

(3)   Calculate the black start recovery index. Update the current optimal solution. Determine whether to analyze all grids in Pareto's non-dominated solution set. If yes, the optimal grid structure will be output; otherwise, skip to 1) and continue searching.

4. Example Analysis

4.1. An Example Analysis of the IEEE (Institute of Electrical and Electronics Engineers)-30 Node System

IEEE-30 node system calculation is used to verify the proposed construction method of the backbone grid structure considering the recovery ability. The power grid structure of IEEE 30 node system is shown in Figure 6. The generator nodes in the IEEE-30 node system include 1, 2, 13, 22, 23 and 27. No. 1 is the node where the black start power is located. The first-level important load nodes are 7, 17, 19 and 21. The rest are the second-level important load nodes. The active and reactive power consumption data of each node are shown in Table A1. Technical parameters of generator set in power grid are shown in Table A2. Technical parameters of lines in power grid are shown in Table A3.
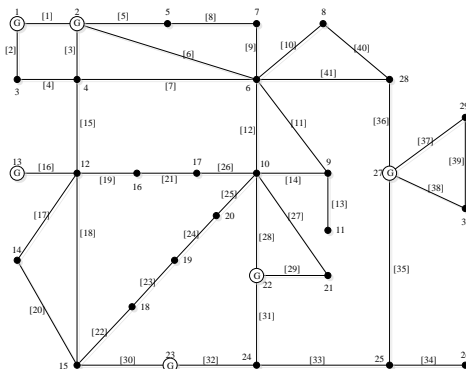

Figure 6. Diagram of the IEEE-30 bus system.

4.1.1. Optimization of the Backbone Grid Structure in the Normal Scenario

In the normal scenario, the solution is based on the method in Section 2. Set the parameters of the discrete particle swarm optimization algorithm as follows: the number of particles is 20, the number of iterations is 100, the inertia coefficient is 1.2, the learning factors are respectively 2 and 2. The PQ (Fast power flow decoupling algorithm) method is used to nest the power flow calculation in the cycle, and three optimal schemes of the multi-objective optimization model are obtained. The non-dominated solution set is shown in Figure 7, and the grid structure is shown in Figure 8.
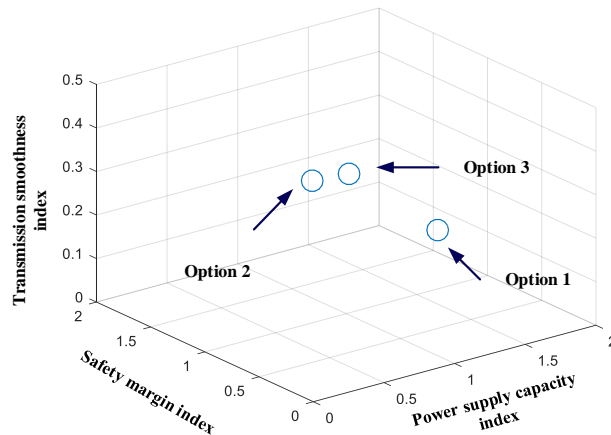

Figure 7. Pareto solutions of the general scheme.

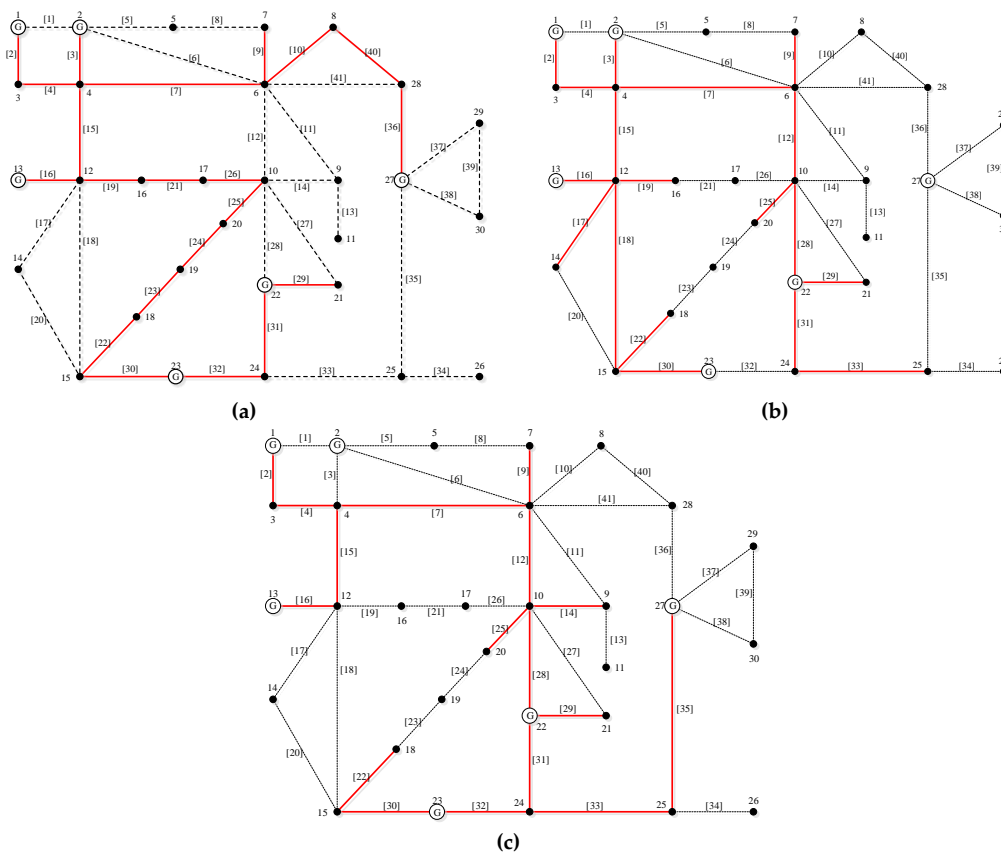(a)

(b)

(c)

Figure 8. Pareto solution set corresponding to the backbone grid structure; (**a**) Option 1 corresponds to the backbone grid; (**b**) Option 2 corresponds to the backbone grid; (**c**) Option 3 corresponds to the backbone grid.

Among the three options, option I has the highest power supply capacity. The corresponding safety margin and unimpeded transmission of option I are relatively low. Option II has the highest unimpeded transmission. The corresponding power supply capacity and safety margin of option II are relatively low. Option III has the highest safety margin. The unimpeded transmission and power supply capacity are relatively low. Only considering the power supply capacity, unimpeded transmission set and safety margin under normal circumstances, schemes 1, 2 and 3 do not dominate each other. We cannot determine the optimal scheme. Meanwhile, it cannot reflect and consider the recovery ability of the backbone grid.

4.1.2. Optimization of the Recovery Performance of the Backbone Grid Considering the Minimum Guarantee

In the power outage scenario, the Pareto non-dominated grid set based on the normal scenario search is used to search for the optimal recovery scheme for the solution concentration scheme with the Dijkstra algorithm, and the search results are shown in Table 1. The best scheme is the one with the largest recovery index value. The optimal grid structure obtained by this method is compared with the optimization method only considering normal scenarios and other search methods for the backbone grid, as shown in Table 2. The optimal grid structure obtained in Lin et al. [26] and Zhou et al. [22] is shown in Figure 9.

**Table 1.** The optimal recovery plan of each alternative backbone grid.

Option	Starting Unit	Optimal Path	Fable	T/min
1	2	1-3-4-2	0.315	116
	13	1-3-4-12-13		
	22	1-3-4-12-16-17-10-20-19-18-15-23-24-22		
	23	1-3-4-12-16-17-10-20-19-18-15-23		
	27	1-3-4-6-8-28-27		
2	2	1-3-4-2	0.427	110
	13	1-3-4-12-13		
	22	1-3-4-6-10-22		
	23	1-3-4-12-15-23		
3	13	1-3-4-12-13	0.392	103
	22	1-3-4-6-10-22		
	23	1-3-4-6-10-22-24-23		
	27	1-3-4-6-10-22-24-25-27		

Table 2. Comparison between the conventional method and the method in this paper.

Grid Construction Considerations	Alternative Program	f1	f2	f3	frec	Optimal Scheme
Optimization in normal scenarios	1	1.81	1.21	0.10	-	Based on focus selection
	2	1.53	1.97	0.15	-	
	3	1.42	1.49	0.23	-	
Increase outage scenario optimization	1	1.81	1.21	0.10	0.083	Option 2
	2	1.53	1.97	0.15	0.207	
	3	1.42	1.49	0.23	0.186	
Method in literature [26]	—	1.62	1.92	0.18	0.153	Option 4
Method in literature [22]	—	1.58	1.83	0.21	0.102	Option 5

According to Tables 1 and 2 and Figure 8, the best scheme is option 2. This can be seen from Tables 1 and 2 and Figure 8. The f_{able} and *T* of option 1 are 0.315 and 116 minutes, respectively. The recovery success rate of the grid structure is relatively low, and the recovery time is long. The reason is that the power supply capacity is sudden, and more load nodes and units are reserved. Unit 22 needs to pass the long path 1-3-4-12-16-17-10-20-19-18-15-23-24-22, involving more lines and transformers, which increases the risk of starting failure caused by inrush current and line overvoltage. At the same time,

there are too many nodes to be recovered, which requires many lines to recover to node 21, greatly delaying the recovery speed. On the other hand, option 2 reduces some generating units and load nodes, so the power supply capacity F1 is 15.5% lower than in option 1. However, no unit can go through too many lines and equipment to startup, so the recovery success rate is increased by 24.4%.

(a)   (b)
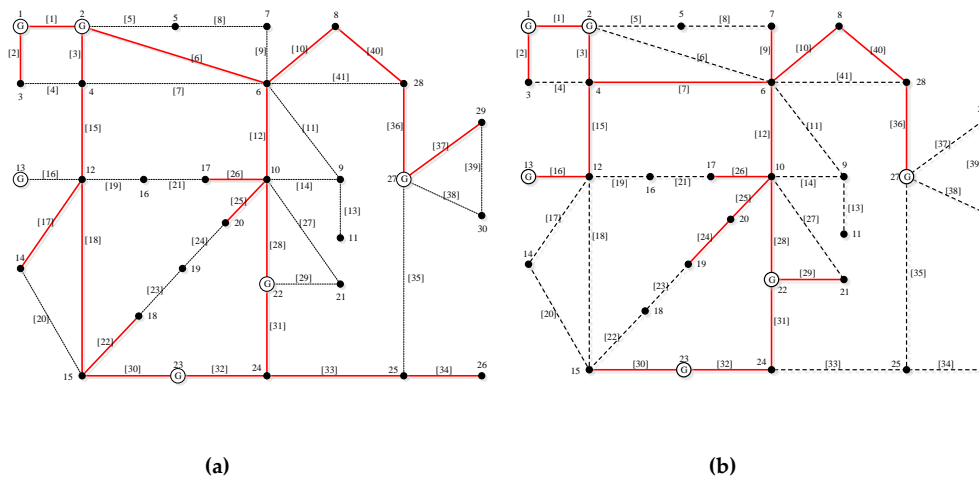
Figure 9. The optimal grid structure obtained by other methods; (**a**) Option 4 corresponds to the backbone grid; (**b**) Option 5 corresponds to backbone grid.

In Zhou et al. [22], multiple indexes are converted into a single index by setting the weight, so as to solve the problem introduced by the fact that multiple objectives cannot determine the unique solution. The option 4 obtained by searching the network is found. In Lin et al. [26], the method focuses more on the risk resistance ability of the grid structure, so the option 5 obtained by searching is more prominent in the indexes f2 and f3, which reflect the safety margin. Compared with the methods proposed in Zhou et al. [22] and Lin et al. [26], there is no significant difference among the three indexes in the normal scenario. In other words, the power supply capacity and safety margin of the important load are equivalent, which verifies the effectiveness of the method in this paper. At the same time, as regards power failure recovery, the method in this paper has a stronger recovery capacity due to considering the factors affecting recovery.

To sum up, compared with just considering the normal scenario, considering the outage scenario can quantitatively reflect the difference in the recovery capacity of different grids. At the same time, the load and unit in the grid structure can be restored by black start power supply through a more reliable and time-consuming path. Finally, it grants the backbone network of the minimum guaranteed grid a good recovery ability on the basis of power supply capacity, safety margin and smooth transmission.

4.2. Comparative Analysis of Different Black Start Power Positions

The black start power supply is one of the important factors affecting the recovery [6]. Set up a comparison scenario. Change the location of the black start power supply to node 22 and compare it with the location of the black start unit at node 1. The results are shown in Table 3. When the black start power supply is located at 22, in option 1, the path is 22-24-23-15-18-19-20-10-17-16-12-4-6-8-28-27 for the black start unit of node 22 to recover the unit located at node 27, which is more difficult to recover than when the black start power supply is located at node 1. For option 3, node 22 is easier to extend to unit nodes 1, 13 and 13 in network topology 23, 27. For option 2, compared with the black start power supply located at node 1, the length of the path between the black start power supply and the unit node does not change much, when the black start power supply is located at node 22. Therefore, the recovery index of option 3 finally exceeds option 2 and becomes the optimal option.

In conclusion, the construction strategy of the core backbone grid structure considering the recovery ability can effectively adjust the optimal option with the change of the equipment parameters affecting the grid structure recovery and the location of the black start power supply.

Table 3. Optimal option for different black start power supply levels.

Black Start Power Node	Alternative Option	f_{rec}	Optimal Option
1	1	0.083	Option 2
	2	0.207	
	3	0.186	
22	1	0.053	Option 3
	2	0.192	
	3	0.201	

4.3. Analysis of an Actual Power Grid Calculation Example

The topological structure of a power grid is shown in Figure 10. The grid consists of 138 nodes and 319 branches, of which 33 nodes contain generators. The black start power supply is at the position shown in the red dot.
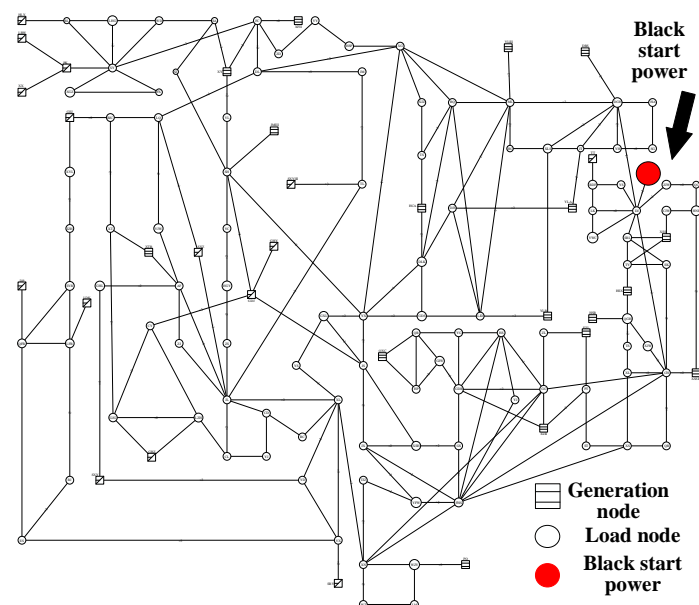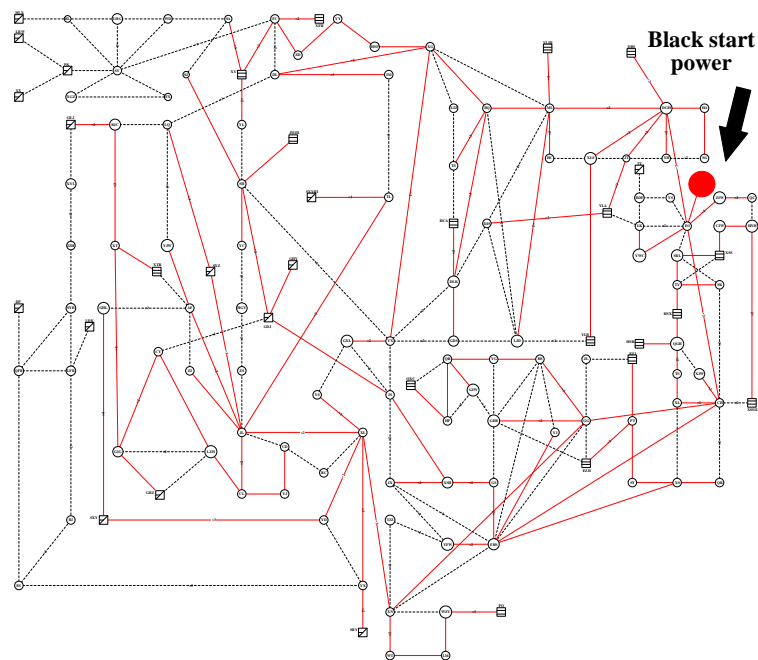

Figure 10. Topological structure of a power grid in Guangdong Province.

By using the method of constructing the core backbone grid structure of the minimum guaranteed power grid considering the recovery ability, all the lines between the nodes corresponding to the optimal backbone grid option are connected. Then, the backbone grid structure of the minimum guaranteed power grid is obtained, as shown in Figure 11, where it is represented by red thick solid lines.

The power saving rate of the optimal option $a_1 = 0.71$. The important load saving rate $a_2 = 0.77$, covering most of the important loads. The node voltage margin $s_1 = 0.86$. The power margin of the generation node $s_2 = 0.27$ and f3 = 0.21, which is a relatively high level. The recovery success rate is 0.96, based on the maximum value of all options, and the total recovery time is 1.12, based on the minimum value of all options, so the recovery ability is good.

From the simulation results of two examples, it can be seen that the optimal option obtained in this paper can improve the recovery ability of a grid structure, in addition to considering the power supply capacity, safety margin and transmission smoothness.

Figure 11. Topological structure of a power grid in Guangdong Province.

5. Conclusions

Based on the electrical parameters reflecting the backbone grid's ability to support important loads, an optimization model with three objectives—power supply capacity, safety margin and transmission smoothness—under a normal scenario was constructed. On this basis, the factors affecting the grid restoration under a power failure scenario were analyzed and the restoration index was quantified. According to the index, the grid structure was reoptimized. The above is the backbone network construction method considering the recovery capacity. The effectiveness of the proposed model and method was verified by an example, and the main conclusions are as follows:

- The proposed strategy can optimize the recovery path of grid units and load nodes. Considering the recovery success rate formed by the line and transformer parameters on the recovery path, it can effectively reduce the nodes involved in too many devices during recovery and reduce the risk of starting failure caused by inrush current or line overvoltage.
- When considering the restoration index in the outage scenario, the scheme in this paper can optimize the comprehensive effect of the recovery time and the recovery success rate of the grid structure. Considering the specific recovery process in the outage scenario, it can effectively reflect the difference of recovery ability between different grid structures and optimize the recovery ability of grid structures according to the recovery index.
- The proposed strategy can effectively adjust the optimal scheme with the change of equipment parameters and the position of the black start power supply.

In the future, the factors that affect the restoration of the grid structure can be further studied.

Conflicts of Interest: The authors declare no conflicts of interest.

Nomenclature

F_{normal}	The Optimal Solution under Normal Power Supply Scenario
f_1, f_2, f_3	the power supply capacity index, the safety margin index, transmission smoothness index
a_1, a_2	the power saving rate, the important load saving rate
β_1	the important load saving rate, a_2 weight
b_g	the total number of generation nodes in the grid
w_k^{bg}	the rated generation capacity of the k-th generation node in the grid
n_g	the total number of generation group nodes in the grid before optimization
w_i^{ng}	the rated generation capacity of the i-th generation node in the grid before optimization
b_l	the total number of load nodes in the grid
w_k^{bl}	the power consumption of the k-th load node in the grid
α_k	the weight of load nodes in the grid, which is selected based on the power user level, so as to distinguish the user importance level
n_l	the total number of load nodes in the grid before optimization
w_i^{nl}	the rated power generation of the i-th power generation node in the grid before optimization
s_1, s_2, β_2	the node voltage margin, the power margin of the generating node, the power margin weight of the generating node
b, r_k^b	the total number of nodes in the grid, the weight of the k-th node in the grid
U_k^*	the voltage margin of the k-th node
$U_{kN}, U_{\max,k}, U_{\min,k}$	the rated voltage of k-th node, the upper limit of the allowable voltage of the k-th node, the lower limit of the allowable voltage of the k-th node
$w_{i,\max}^{bg}$	the maximum active power output of the i-th generation node in the grid structure.
n_{path}	the number of reserved lines in the grid
$r_k^{path}, P_{k,\max}^{path}, P_k^{path}$	the weight of the k-th line in the grid, the active power transmission limit of the k-th line in the grid, the active power transmission of the k-th line in the grid in the normal power supply scenario
$X = (X_1, X_2, \cdots, X_n)$	Initialization of particle swarm
$X_i = (x_{i1}, x_{i2}, \cdots, x_{id})$	the position coordinate of each individual in particle swarm, the value of each dimension of the position variables of all particles x_ik is limited to 0 or 1.
$V_i(v_{i1}, \ldots, v_{id})$	the flight speed of particle i
$P_i(p_{i1}, p_{i2}, \ldots, p_{id})$	The optimal location of particle i
$P_g(p_{g1}, p_{g2}, \ldots, p_{gd})$	the optimal location of particle swarm
w	the inertial coefficient, with the value range generally taken as $0.4 < w < 1.4$;
c_1, c_2	the learning factor
r_1, r_2	random numbers in the [0,1] interval.
F_{black}	the optimal solution in case of power failure
f_{rec}	the recovery index.
f_{able}	the recovery success rate
$\beta_3,$	the total recovery time, the total recovery time weight
Φ	the set of paths
W_{Li}, W_{T_k}, L_i	Line index, transformer index, the optimal recovery path of the generator set i to be recovered
$X_{Cj}, X_{C\max}$	the equivalent capacitive reactance of the branch j in the path, the maximum capacitive reactance value of all lines
$\phi_{\mathrm{sat}k}, \phi_{\mathrm{res}k}, \phi_{mk}$	the saturation flux of the transformer
T_1, T_2	the time required to start the unit in the first step, the time required to recover the remaining nodes in the second step
t_j^L, t_k^G, t_{black}	the charging time of the j-th line included in the path, the starting time of the k-th station included in the path, the starting time of the black start unit
q_i	the equivalent length of line i
$L_{\max}$	the longest path between the unrecovered node and the recovered node
P_k^G, w_k^{bg}	the climbing rate of the k-th generation node, the output of the k-th generation node after system recovery

Appendix A

Table A1. IEEE30 bus data.

Bus Number	Pd	Qd	Vmax	Vmin	Load Importance Level
1	0	0	1.05	0.95	-
2	21.7	12.7	1.1	0.95	-
3	2.4	1.2	1.05	0.95	2
4	7.6	1.6	1.05	0.95	1
5	0	0	1.05	0.95	3
6	0	0	1.05	0.95	3
7	22.8	10.9	1.05	0.95	1
8	30	30	1.05	0.95	1
9	0	0	1.05	0.95	3
10	5.8	2	1.05	0.95	2
11	0	0	1.05	0.95	3
12	11.2	7.5	1.05	0.95	2
13	0	0	1.05	0.95	–
14	6.2	1.6	1.05	0.95	1
15	8.2	2.5	1.05	0.95	1
16	3.5	1.8	1.05	0.95	2
17	9	5.8	1.05	0.95	2
18	3.2	0.9	1.05	0.95	1
19	9.5	3.4	1.05	0.95	2
20	2.2	0.7	1.05	0.95	1
21	17.5	11.2	1.05	0.95	2
22	0	0	1.05	0.95	–
23	3.2	1.6	1.05	0.95	–
24	8.7	6.7	1.05	0.95	1
25	0	0	1.05	0.95	3
26	3.5	2.3	1.05	0.95	1
27	0	0	1.05	0.95	–
28	0	0	1.05	0.95	3
29	2.4	0.9	1.05	0.95	1
30	10.6	1.9	1.05	0.95	2

Notes: baseMVA = 100, Unit value is used in the Table.

Table A2. IEEE30 generator data.

Bus Number	Maximum Output (MW)	Unit Capacity (MW)	Climbing Rate (MW/min)	Startup Time (min)
1	80	100	10	30
2	80	100	10	25
22	50	100	8	30
27	55	100	8	30
23	30	100	3.5	25
13	40	100	5	25

Table A3. IEEE30 branch data.

From Bus	To Bus	r	x	b	Allowable Capacity of Long-Distance Transmission Branch (MVA)	Charging Time (min)
1	2	0.02	0.06	0.03	130	8
1	3	0.05	0.19	0.02	130	8
2	4	0.06	017	0.02	65	5
3	4	0.01	0.04	0	130	8
2	5	0.05	0.2	0.02	130	8
2	6	0.06	0.18	0.02	65	5
4	6	0.01	0.04	0	90	7

Table A3. *Cont.*

From Bus	To Bus	r	x	b	Allowable Capacity of Long-Distance Transmission Branch (MVA)	Charging Time (min)
5	7	0.05	0.12	0.01	70	6
6	7	0.03	0.08	0.01	130	8
6	8	0.01	0.04	0	32	4
6	9	0	0.21	0	65	5
6	10	0	0.56	0	32	4
9	11	0	0.21	0	65	5
9	10	0	0.11	0	65	5
4	12	0	0.26	0	65	5
12	13	0	0.14	0	65	5
12	14	0.12	0.26	0	32	4
12	15	0.07	0.13	0	32	4
12	16	0.09	0.2	0	32	4
14	15	0.22	0.2	0	16	3
16	17	0.08	0.19	0	16	3
15	18	0.11	0.22	0	16	3
18	19	0.06	0.13	0	16	3
19	20	0.03	0.07	0	32	4
10	20	0.09	0.21	0	32	4
10	17	0.03	0.08	0	32	4
10	21	0.03	0.07	0	32	4
10	22	0.07	0.15	0	32	4
21	22	0.01	0.02	0	32	4
15	23	0.1	0.2	0	16	3
22	24	0.12	0.18	0	16	3
23	24	0.13	0.27	0	16	3
24	25	0.19	0.33	0	16	3
25	26	0.25	0.38	0	16	3
25	27	0.11	0.21	0	16	3
28	27	0	0.4	0	65	5
27	29	0.22	0.42	0	16	3
27	30	0.32	0.6	0	16	3
29	30	0.24	0.45	0	16	3
8	28	0.06	0.2	0.02	32	4
6	28	0.02	0.06	0.01	32	4

References

1. Sun, H.D.; Xu, T.; Guo, Q.; Li, G.F. Analysis on Blackout in Great Britain Power Grid on August 9th, 2019 and its Enlightenment to Power Grid in China. *Proc. CSEE* **2019**, *21*, 1–11.
2. Yi, J.; Bu, G.Q.; Guo, Q. Analysis of "3.21" blackout in Brazil and Its Enlightenment to China Power Grid. *Power Syst. Autom.* **2019**, *43*, 7–15.
3. Lin, W.F.; Guo, Q.; Yi, J. Analysis on Blackout in Argentine Power Grid on June 16, 2019 and Its Enlightenment to Power Grid in China. *Proc. CSEE* **2020**. [CrossRef]
4. Mariani, E.; Mastroianni, F.; Romano, V. Field Experiences in Reenergization of Electrical Networks from Thermal and Hydro Units. *IEEE Trans. Power Appar. Syst.* **1984**, *PAS-103*, 1707–1713. [CrossRef]
5. Salvati, R.; Sforna, M.; Pozzi, M. Restoration project Italian power restoration plan. *IEEE Power Energy Mag.* **2004**, *2*, 44–51. [CrossRef]
6. Liu, Y.T.; Wang, H.T.; Ye, H. *chapter one. Theory and Technology of Power System Restoration*; Science Press: Beijing, China, 2014; Volume 3, pp. 1–58.
7. Zhang, S. *Simulation Model and Risk Assessment of Power System Blackout*; North China Electric Power University, Post-Graduate: Baoding, China, 2010.
8. Gu, X.P.; Yang, C.; Liang, H.P.; Li, S.Y. Path Optimization of Power System Restoration With HVDC Transmission. *Power Syst. Technol.* **2019**, *43*, 2020–2032.
9. Kun, J.T.; Shu, S.D.; Yu, Q.L. Asynchronous distributed global power flow method for transmission–distribution coordinated analysis considering communication conditions. *Electr. Power Syst. Res.* **2020**, *182*, 106256.

10. Feng, S.; Yi, Z.; Gang, W. Study on charging and discharging characteristics of energy storage system in wind storage power plant under the condition of black start. *Adv. Mater. Res.* **2015**, *1070*, 443–448.

11. Majid, E.M.; Hamid, F.; Mahdi, F. A Novel Method of Optimal Capacitor Placement in the Presence of Harmonics for Power Distribution Network Using NSGA-II Multi-Objective Genetic Optimization Algorithm. *Sustainability* **2020**, *10*, 2344.

12. Damir, J.; Josip, V.; Petar, S. Optimal Reconfiguration of Distribution Networks Using Hybrid Heuristic-Genetic Algorithm. *Sustainability* **2020**, *13*, 1544.

13. Pei, Z.; Yang, L.W.; Li, K.L. Short-Term Wind Power Prediction Using GA-BP Neural Network Based on DBSCAN Algorithm Outlier Identification. *Sustainability* **2020**, *8*, 157.

14. El-Zonkoly; Amany, M. Renewable energy sources for complete optimal power system black-start restoration. *IET Gener. Transm. Distrib.* **2015**, *9*, 531–539. [CrossRef]

15. Fei, L.P.; Jun, L.; Ben, D.T. Stacked-GRU Based Power System Transient Stability Assessment Method. *Sustainability* **2020**, *11*, 121.

16. GU, M.H.; Sun, W.B.; Li, P.P. Evaluation Index System for Urban Elastic Distribution Network in the Face of Extreme Disturbance Events. *Proc. CSU-EPSA* **2018**, *7*, 103–109.

17. Dong, F.F.; Liu, D.C.; Wu, J. A Method of Constructing Core Backbone Grid Based on Improved BBO Optimization Algorithm and Survivability of Power Grid. *Proc. CSEE* **2014**, *34*, 2659–2667.

18. Zhu, H.N.; Liu, Y.T.; Qiu, X.Z. Optimal Restoration Unit Selection Considering Success Rate during Black StartStage. *Autom. Electr. Power Syst.* **2013**, *22*, 34–40.

19. Feng, L.; Jin, L.M.; Zhang, T.Z. Optimal Restoration Unit Selection Considering Success Rate during Black StartStage. *Proc. CSEE* **2016**, *36*, 4904–4910.

20. Zhao, Y.X.; Han, C.; Lin, Z.Z. Two-stage Core Backbone Network Optimization Strategy for Power Systems with Renewable Energy. *Power Syst. Technol.* **2019**, *43*, 16–31.

21. Huan, J.J.; Wei, B.; Sui, Y. A Multi-Objective Planning Method of Urban Secure Power Networks Guaranteed Against Typhoon and Disaster. *Power Syst. Technol.* **2018**, *15*, 12–25.

22. Zhou, Z.; Lei, L.; Wu, H.B. Study on Survivability Evaluation of Core Backbone Network Based on Multiple Indexes Synthesis Method. *Smart Power* **2018**, *6*, 1–6.

23. Bi, T.Z.; Huang, S.F.; Xue, A.C. An Approach for Critical Lines Identification Based on the Survivability of Power Grid. *Proc. CSEE* **2011**, *7*, 31–37.

24. Golshani, A.; Sun, W.; Zhou, Q. Incorporating wind energy in power system restoration planning. *IEEE Transactions on Smart Grid* **2019**, *10*, 16–28. [CrossRef]

25. Fu, Z.H. *Network Reconstruction and Partition Restoration Strategy in Power System Restoration*; Zhejiang University, Post-Graduate: Hangzhou, China, 2017.

26. Lin, X.; Liu, Y.; Xu, L.X. A method of searching backbone grid based on survivability of power system. *Electr. Meas. Instrum.* **2019**, *12*, 49–56.